24th COBEM - 2017

24th ABCM International Congress of Mechanical Engineering
December 3-8, 2017, Curitiba, PR, Brazil

COBEM-2017-1152
CONCEPTION AND EVALUATION OF A TRACKING SYSTEM FOR A LINEAR FRESNEL CONCENTRATOR

Pedro Milanez Brogni
João Pedro Grobberio Trancoso
Gabriel Mendes Cascaes
Victor César Pigozzo Filho
Alexandre Bittencourt de Sá
Júlio César Passos
Universidade Federal de Santa Catarina - Campus Reitor João David Ferreira Lima, s/n - Trindade, Florianópolis - SC, 88040-900
pedro_brogni@hotmail.com, jp.grobbeiro@gmail.com, jp.grobbeiro@gmail.com, gabrielcascaes_g_@hotmail.com, victorpigozzo@gmail.com, alexandre.sa@lepten.ufsc.br, Julio.passos@ufsc.br

Abstract. *The solar tracking system is a main component of a solar concentrator. A tracking mechanism is proposed and tested under real conditions in a linear Fresnel concentrator prototype at LEPTEN/UFSC with 54m² of mirror area. The receiver is 150mm wide and it is located 3,75m above the mirror field. Analytical and visual tests were performed to verify the accuracy obtained with the tracking device. The Solar Position Algorithm (SPA) provided by the NREL is used to provide the sun position. The maximum uncertainty obtained for the solar transversal incidence angle was 0.0607°. For positioning the mirrors the uncertainties varied from 0.07 to 0.12 depending on the solar transversal incidence angle.*

Keywords: *Solar Energy, Linear Fresnel Concentrator, Solar Tracking, Renewable Energy*

1. INTRODUCTION

Concentrated solar power (CSP) is one of most promising renewable energy source for a near future. According to the roadmap developed by the International Energy Agency, CSP is expected to generate 11% of global electricity generation by 2050 (Philibert, 2014).

There are four main types of CSP technologies, two of punctual focus: solar towers and parabolic dish; and two of linear focus: Parabolic Trough Concentrator (PTC) and Linear Fresnel Concentrator (LFC). The parabolic trough is the most developed and used CSP technology. The LFC is a growing technology that presents some advantages (Barlev et al., 2011; Morin et al., 2012) such as lower costs and simplicity by using flat mirrors. LFC seem to be the best concentration technology for steam generation up to 200°C, which includes most of industrial process heat applications (Morin, et al., 2012). The feasibility of the direct steam generation (DSG) process in PTC has been already proved in the DISS project (Zarza et al., 2004), and now efforts are being made in assessing the reliability for DSG in LFC.

The LFC consists of parallel mirror lines that reflect the sun radiation to the receiver. The receiver is fixed above the mirror field and as the sun moves, the mirrors lines need to track the sun to correct its position and reflect it to the receiver. A single tracking device can be used for each line or one common tracking device for the all the mirror lines. The first provides a better controllability and optimization possibilities and the latter provides a much simpler and more cost-effective option and are more common in small size LFC (Guangdong, et al., 2014).

The team of the LEPTEN laboratories, at the Federal University of Santa Catarina (UFSC), has developed a linear Fresnel concentrator prototype (Fig. 1). The project objective is to study a small scale LFC operating at DSG. One of the many tasks performed under this project included the development and evaluation of the solar tracking and mirror positioning system for the prototype. The optical efficiency and feasibility of the LFC is highly dependent on the accuracy of the tracking system.

The objective of this work is to evaluate how all the sources of uncertainties affect the angular positioning of the mirrors lines, and its consequence at the optical performance of the LFC. A sensibility analysis showed which uncertainties have the higher influence on the overall uncertainty, highlighting the critical parameters for the solar tracking.

Figure 1 – Experimental setup

2. EXPERIMENTAL SETUP AND METHODOLOGY

The analyzed LFC has an area of 60m² and it's used for research in direct steam generation project. The mirrors are arranged in 10 lines of 12m in length and 0.45m wide. The absorber is a trapezoidal cavity with six parallel tubes of 25,4mm each and it is positioned at 3,75m above the mirrors. The prototype is installed at the Federal University of Santa Catarina in the city of Florianopolis, south Brazil.

2.1 Linear Fresnel Concentrator Tracking Mechanism

As the position of the Sun changes in the sky throughout the day the mirror lines angular position must be corrected to continuously reflect the solar radiation into the absorber. Figure 2 shows the tracking mechanism, composed of ten parallel lever arms, one for each line, connected by the actuator bar.

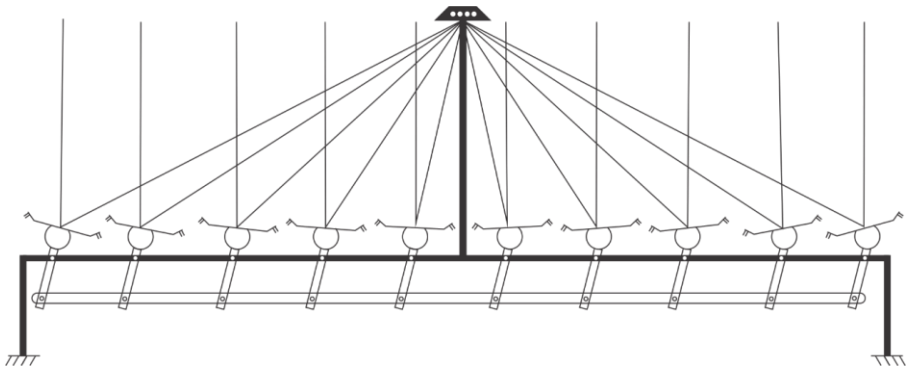

Figure 2 – Tracking mechanism schematics

In Fig. 3 the linear actuator is shown connected to the actuator bar. The tracking mechanism must be very robust and tight, to avoid looseness in the rotating joints and keep a position still without vibration. The projected mechanism is capable of rotating the mirror lines by 80°, tracking the sun almost the entire day, form -80° to 80° in the solar transversal incidence angle, θ_T . The linear actuator has a low speed and a high torque. A PWM speed controller was used to decrease even more the speed of the actuator, increasing the position controllability accuracy.

Figure 3 – Tracking mechanism

Inclinometers are used to measure the inclination of the lever arms and consequently the angular position of the mirror lines. The inclinometer is installed at the second line of the collector.

2.2 Solar Tracking Angles

The position of the Sun can be found through solar equations, which depends on current time, location and other aspects. For this work, the solar azimuth and zenith angles were found using the algorithm developed by the National Renewable Energy Laboratory (NREL, 2017), which have an accuracy of ± 0,0003° (Reda and Andreas, 2008). This information is crucial for defining and controlling the inclination of the mirrors in order to correctly focus the solar radiation on the receiver. Figure 4 explains the relation between the solar vector and angles with the main angles presented on a LFC.

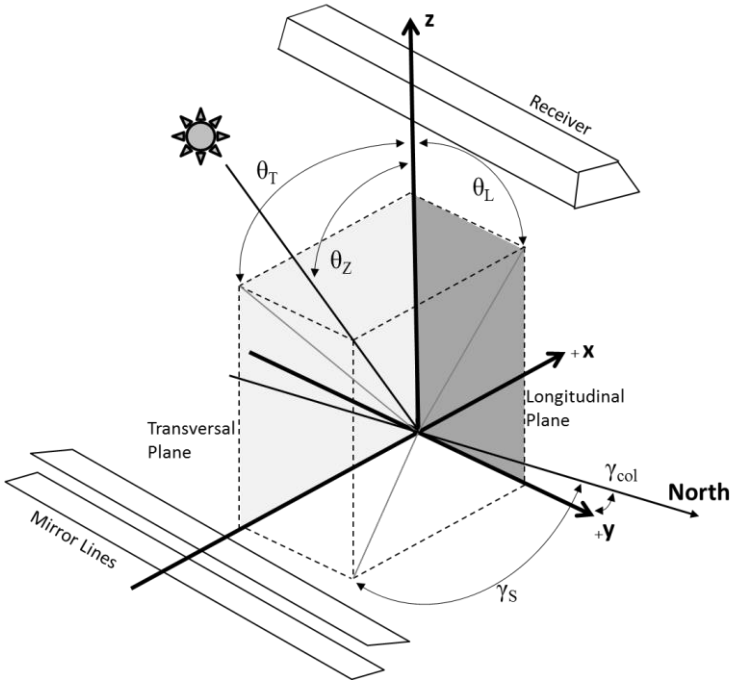

Figure 4 – Solar angles and reference angles for a linear Fresnel concentrator

The solar vector is defined by two angles, the zenith and the azimuth. The zenith angle (θ_Z) relates the direction of the sun with the zenith axis, which is a vector perpendicular to the horizontal plane, and it is represented in Fig. 4 by the

z axis. The solar azimuth angle (γ_s) is the angle between the solar vector projection on the horizontal plane and the north axis. This angle is positive when shifting to west, and negative to east, going from -180 to 180°. It is noteworthy that our workbench follows the same orientation as the building where it is installed, which has a small deviation from the north south axis. The collector azimuth angle (γ_{col}) represents this deviation, relating the collector axis with the true north axis, using the same notation as the azimuth angle.

These angles are used to find two important angular relations that characterize the LFC. The solar incident transversal angle (θ_T), which is the inclination between the solar vector projection on the transversal plane of the collector with the zenith, and the solar longitudinal incidence angle (θ_L), that is the inclination between the solar vector projection on the longitudinal plane of the collector with the zenith. The solar notation adopted consider both angles zero when their projection meets the zenith, and they go from -90 to 90°. The θ_T angle is negative in morning, zero at solar noon and positive in the afternoon. Both θ_T and $\theta_L$angles are found using Equations (1) and (2).

$$\theta_T = \tan^{-1}[\tan\theta_Z \ .\sin(\gamma_s - \gamma_{col})] \quad (1)$$

$$\theta_L = \tan^{-1}[\ \tan\theta_Z \ .\cos(\gamma_s - \gamma_{col})] \quad (2)$$

The LFC tracks the Sun in just one axis and as the mirror lines are parallel to the absorber, only the transversal angle is important for solar tracking. Its relation with the mirror positioning is described in Fig. 5.

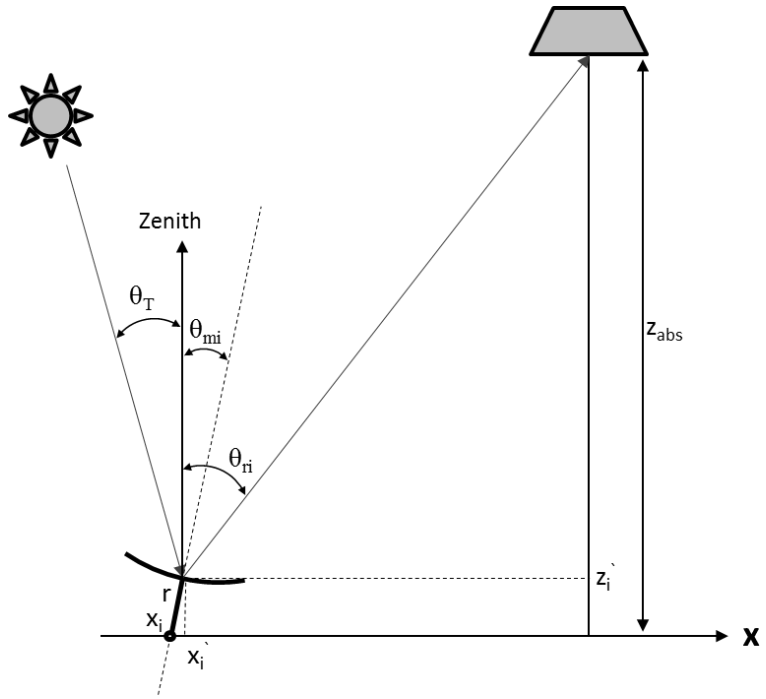

Figure 5 – Mirror position angular relations

The mirror angle (θ_{mi}) is the position that the i^{th} mirror line must be in order to reflect the solar radiation in the middle of the absorber. The reflected radiation angle (θ_{ri}) defines the angle between the center of the mirror to the center of the absorber. The position of the center of rotation for each mirror line is given by x_i. The mirrors reflective surface center has a radius distance, *r*, of 65mm. The positions x_i' and z_i' indicates the real position of the center of the mirrors.

The following transcendental Equations (3) and (4) must be solved in order to find the mirror angular position of each mirror line.

$$\theta_{ri} = \tan^{-1}\left(\frac{-x_i - r\sin\theta_{mi}}{Z_{abs} - \ r\cos\theta_{mi}}\right) \quad (3)$$

$$\theta_T = 2\theta_{mi} - \theta_{ri} \quad (4)$$

These equations were solved for a transversal angle varying from -80° to 80°, which includes all the working hours of the workbench. This is called the exact mirror position solution. The results for each line were than linearized to

obtain an equation like Equation (5), with the coefficients showed in Table 1. The parameter "a" represents the angular pace that the mirrors move regarding the transversal angle, while the "b" parameter represents the initial offset that all mirrors have in relation to each other.

$$\theta_{mi} = a\,\theta_T + b \tag{5}$$

Table 1. Angular pace, *a*, and offset, *b*, for each mirror line

	mirror line									
	1	**2**	**3**	**4**	**5**	**6**	**7**	**8**	**9**	**10**
a	0.4966	0.4963	0.4961	0.4959	0.4958	0.4958	0.4959	0.4961	0.4963	0.4966
b	15.8311	12.8113	9.4542	5.8066	1.9593	-1.9594	-5.8066	-9.4543	-12.8113	-15.8312

If the rotating radius of the mirrors, *r*, were zero, all the mirror lines would have the same angular coefficient *a* equal to 0.5, which means that in this case, all the mirror lines of the LFC rotates at the same rate, which is half of the solar transversal angle incidence variation.

For the analyzed case the mirror lines do not rotate at the same rate, and as a single tracking mechanism is being used it causes errors in the mirror positioning. These errors were all evaluated.

2.3 Uncertainty Sensibility Analisys

The experiment undertook intends to find the final uncertainty of mirror's position (θ_{mi}). Figure 6 shows photos of the receiver under the focus of the second mirror lane, which is where the inclinometers are installed. Sheets of paper with stripes drawn on it were attached to the glass window on the bottom of the receiver, in order to facilitate seeing the concentrated radiation. The middle stripe indicates the middle of the receiver, and the two other stripes contains the area of the absorber elements. As seen in the photos a, b c and d from Fig. 6, even a small shift in the mirror angle results in a deviation of the reflected radiation. Variations in the order of 0.5° can almost totally dislocate the concentrated radiation from the absorber elements. This states the importance of having a good accuracy on the mirror position prediction and measurement.

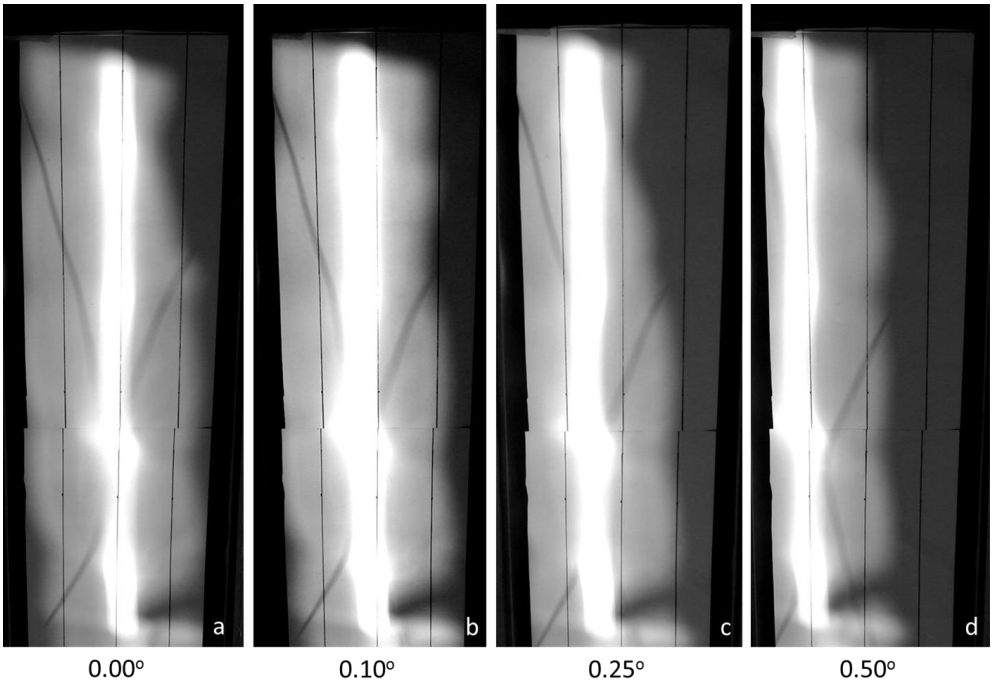

Figure 6 – Visual verification of concentration from second mirror line for different θ_{mi}

Calculating this error requires the knowledge of uncertainty in the solar position on the transversal plane (θ_T) and in the linear and angular coefficient, as shown in Eq. (5).

The method used to obtain the uncertainty of θ_T is based on calculating the maximum combined standard uncertainty throughout each day studied. In this case, the analysis was made for three different days of the year, the winter and summer solstices and fall equinox.

Equation (6) represents θ_T's uncertainty as the propagation of solar zenith and azimuth uncertainties and the collector azimuth angle uncertainty. This method of uncertainty propagations is described by (Holman, 1989). The uncertainty in solar angles, Equations (7) and (8), consider the error individually caused by each parameter used in the solar position algorithm, shown in Table 2.

$$\mu\theta_T = \sqrt{\left(\frac{\partial\theta_T}{\partial\theta_Z}\,\mu\theta_Z\right)^2 + \left(\frac{\partial\theta_T}{\partial\gamma_s}\,\mu\gamma_s\right)^2 + \left(\frac{\partial\theta_T}{\partial\gamma_{col}}\,\mu\gamma_{col}\right)^2} \tag{6}$$

$$\mu{\theta_z}^2 = \mu\, {lat_{\theta_z}}^2 + \mu\, {lon_{\theta_z}}^2 + \mu\, {e_{\theta_z}}^2 + \mu\, {T_{\theta_z}}^2 + \mu\, {P_{\theta_z}}^2 + \mu\, {t_{\theta_z}}^2 \tag{7}$$

$$\mu{\gamma_s}^2 = \mu\, {lat_{\gamma_s}}^2 + \mu\, {lon_{\gamma_s}}^2 + \mu\, {e_{\gamma_s}}^2 + \mu\, {T_{\gamma_s}}^2 + \mu\, {P_{\gamma_s}}^2 + \mu\, {t_{\gamma_s}}^2 \tag{8}$$

Table 2. Uncertainty driven by each individual parameter used in the solar position algorithm

Variable	Value	Uncertainty
Latitude (lat)	-27.6013°	0.0005°
Longitude (lon)	-48.5184°	0.0005°
Elevation (e)	30 m	20 m
Annual avg. local pressure (P)	1010 mbar	50 mbar
Annual avg. local temperature (T)	20°C	10°C
Local time (t)	Current time	10 s

The latitude and longitude numerical value and its uncertainty was found through a conservative approach based on common GPS measurements and Google Maps evaluation. A 0.0005° variation in latitude or longitude represents 55m of position precision. The average pressure and temperature was taken from the National Institute of Meteorology (INMET, 2017). The SPA calculates the solar and azimuth angles for each second in time. The uncertainty of the computers clock that runs the algorithm was taken as a conservative value of 10 seconds.

As seen in Table 1, each mirror lane has one angular pace and offset, however, the tracking mechanism uses only one motor to move all mirror lines. The offset can be set individually for each mirror lane, but the angular pace has to be the same for all lanes. The systematic error that this consideration brings to the mirror position is analyzed at the results section.

Although the values of the linear coefficient "b" were found in Table 1, the experimental setup does not include inclinometers in all the mirror lanes. Therefore, this parameter is established through visual adjustment on initial position for each line of mirrors at solar noon. The uncertainty adopted for this regulation is assumed as 0.05°, which is the half of the smallest increment in reflection's position showed in Figure 6.

3. RESULTS

The sensitivity analysis results of the influence of the SPA inputs on the Zenith (θ_Z) and on the Solar Azimuth angle (γ_s) is shown on Table 3. For each variable, the result showed represent the maximum of the three analyzed days for the entire days. For example, the uncertainty of 0.0005° in the latitude causes at the worst case an uncertainty on the solar azimuth angle of 0.0002°. The latitude and longitude uncertainties influence are small and almost constant during the day and for the three analyzed days.

The annual average pressure and temperature uncertainties have no influence on the solar azimuth angle but increases the uncertainty at the zenith angle. The pressure and temperature are used at the algorithm to calculate the atmospheric refraction of the solar radiation. Their influence at the uncertainty of the zenith angle is higher at high zenith angles, in beginning and end of the days.

The local time uncertainty, of 10 seconds, has the major influence in the both zenith and azimuth angles. Table 3 shows the maximum values but as is shown at Fig. 7, these peaks happen at different moments for each angle. In that matter, combining these two maximums values would overestimate the transversal angle uncertainty.

Table 3 – maximum uncertainty influence of the inputs on the solar position algorithm

	$\mu\theta_z$ [°]	$\mu\gamma_s$ [°]
Latitude	0.0005	0.0002
Longitude	0.0004	0.0006
Elevation	0.0000	0.0000
Annual avg. local pressure	0.0050	0.0000
Annual avg. local temperature	0.0036	0.0000
Local time	0.0309	0.0492

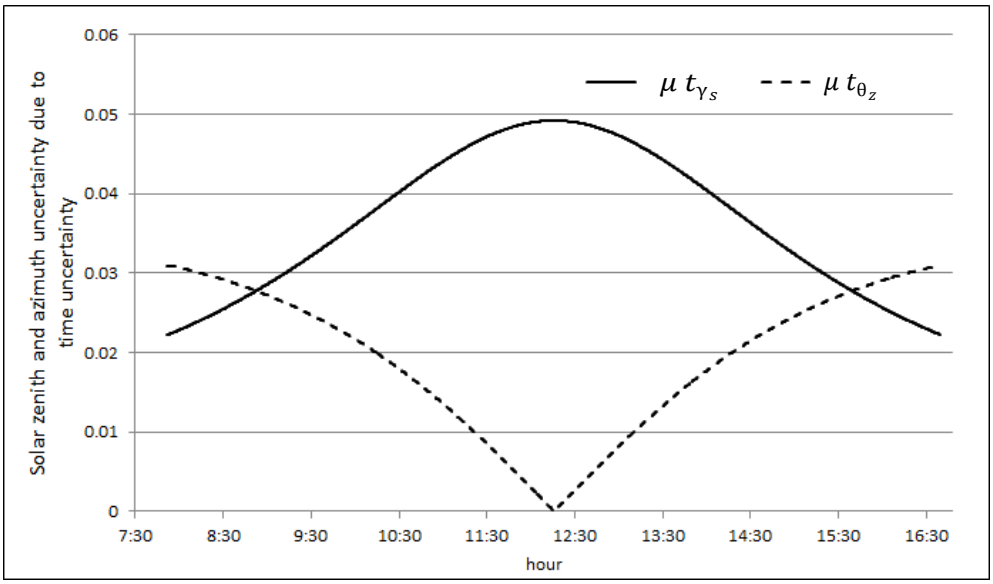

Figure 7 – Influence of time uncertainty on the uncertainties of azimuth and zenith throughout the day

To avoid the overestimation of the solar zenith and azimuth angle, by combining values of different moments, equations 7 and 8 were solved for every instant. Table 4 shows the overall uncertainty for the two solar angles, the solar zenith and azimuth, considering the combined influence of the parameters analyzed.

Table 4 – Overall uncertainty for solar zenith and azimuth angles

	$\mu\theta_z$	$\mu\gamma_s$
Total	0.0316	0.0492

The same approach was used to find the influence of the two solar angles uncertainties found above, for the uncertainty of the transversal angle θ_T, where equation 6 was solved for every instant. The uncertainty of the azimuth of the collector (γ_{col}) has a great influence on the transversal angle. Due to its importance a separated analysis is being performed to assess the orientation of the collector with high reliability. Therefore, for this work the azimuth of the collector was considered as -4.6°, and free of uncertainties.

Figure 8 summarizes the evolution of the zenith, azimuth and the solar transversal incidence angle uncertainties along the day for the worst case day, which is the winter solstice, june 21st. The maximum uncertainty obtained for θ_T is at midday and has a value of 0,0607°.

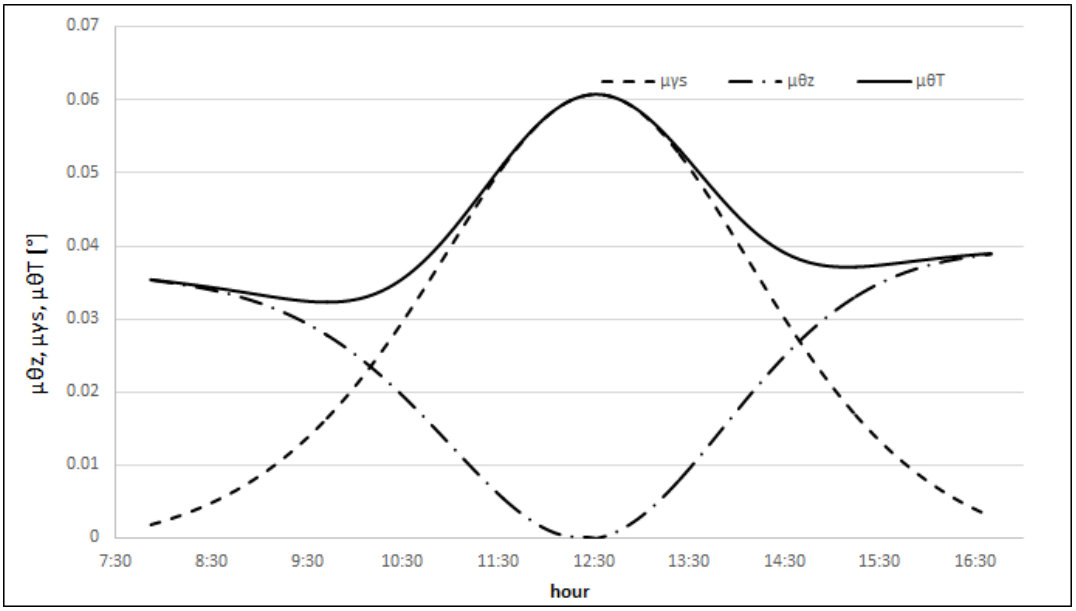

Figure 8 – Influence of the azimuth and zenith angles uncertainty on the combined uncertainty of the transversal angle at the june 21st

As the LFC uses a single mechanism to move all the mirror lines at the same rate of change, a single angular pace must be chosen to be used by the solar tracking system. The tracking equations (Equations (3) and (4)) give the exact position that each mirror line would have if they had separated movement from other lines. The uncertainty of the linearization compares this exact position to the position obtained from the linearization (Eq. (5)), for θ_T ranging from -80° to 80°. This is not an aleatory error, but a systematic error that has to be minimized.

For each θ_T, each mirror line has it's own linearization error. Figure 9 shows the maximum linearization error between the ten lines. It´s important to notice that at low $\theta_T$values, which is the most important operation conditions for tests, the error is smaller.

The angular pace obtained that minimizes the maximum error between all the lines for each θ_T is 0,4962, which is the average value for "a" in Table 1.

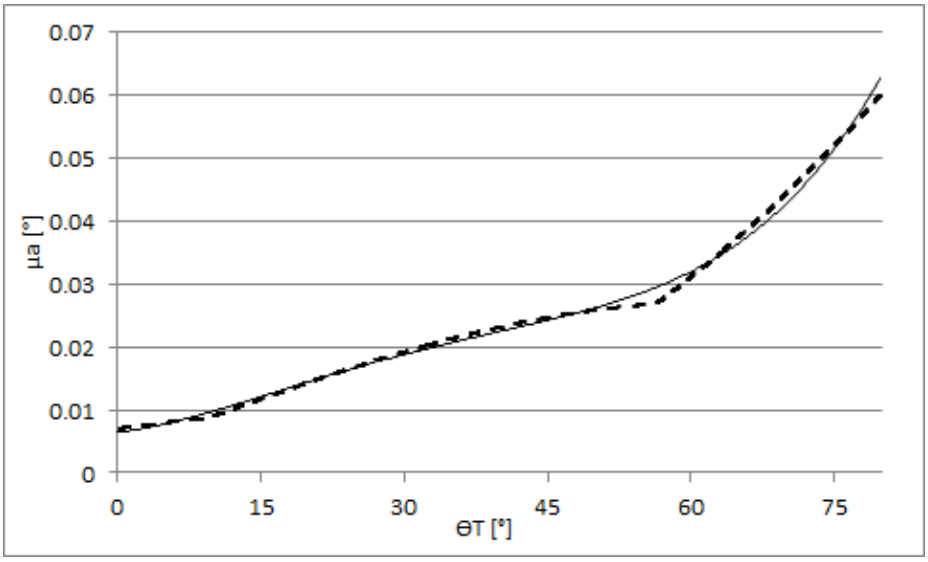

Figure 9 – Maximum linearization error between the mirror lines

Again, in order to not overestimate the importance of the linearization error in the uncertainty of the mirrors position, the maximum value was not used. Instead, the systematic error was expressed as a function of θ_T, as showed

in Eq. (9). In that way, the more relevant test periods, at low transversal angles, are not penalized by the uncertainties of higher transversal angles.

$$\mu\, a = \ 4.89E^{-9}{\theta_T}^4 - 5.58E^{-7}{\theta_T}^3 + 1.98E^{-5}{\theta_T}^2 + 1.90E^{-4}\theta_T + 6.39E^{-3} \quad (9)$$

The total uncertainty for the mirror angle can be calculated using Eq. 10, where μa is the systematic linearization error, and the other part inside the roots is the aleatory error, caused by the uncertainties the offset angle (b), solar incident transversal angle (θ_T), and the inclinometer uncertainty (μ_{inc}). The aleatory error obtained is 0.06°.

$$\mu\theta_M = \mu\, a + \sqrt{(a\, \mu\theta_T)^2 + \mu\, b^2 + \mu\, inc^2} \quad (8)$$

Combining the systematic and the aleatory error it can be stated that the maximum error of positioning the mirror occurs at the beginning and end of the days and has a value of 0.12°. For the period of θ_T going from -45° to 45°, which is the most important operational period, the maximum error of positioning the mirror is 0.085°.

4. CONCLUSIONS

Several experimental tests were performed, where one mirror line tracks the sun during the day. Mirrors from adjacent rows were removed to prevent shading. The concentrated radiation from the curved mirrors stayed on the center of the receiver for the whole day, with no visible deviation. This indicates that the solar tracking equations and the tracking system are both working with satisfactory performance. In addition, it seems that the maximum angular position error obtained is coherent with the experimental results. The robust structure is able to maintain the solar focus even in windy periods.

This was an important step on the development of an operational DSG linear Fresnel concentrator workbench. Further, the behavior of all the lines working together will be investigated. Also, the optical performance will be evaluated in order to characterize the collector before running test with two phase flow. For that, water at ambient temperature will flow through the receiver with all mirror lanes tracking. This configuration reduces thermal losses and will allow quantifying the optical performance of the LFC prototype.

5. ACKNOWLEDGEMENTS

This work was supported by CNPq under the project Heliotérmica CNPq (Proc. 406357/2013-7). The authors also make acknowledgements to CAPES and POSMEC.

6. REFERENCES

Barlev, D., Vidu, R. and Stroeve, P., 2011. Innovation in concentrated solar power. Solar Energy Materials and Solar Cells, 95(10), pp.2703-2725.

Holman, J.P. Experimental methods for engineers. Mcgrall-Hill 5th Ed., Singapure, 1989.

INMET, 2017. “Brazilian National Institute of Meteorology” 19 Sep. 2017 <http://www.inmet.gov.br/portal/>.

Morin, G., Dersch, J., Platzer, W., Eck, M. and Häberle, A., 2012. Comparison of linear Fresnel and parabolic trough collector power plants. Solar Energy, 86(1), pp.1-12.

NREL, 2017. “Solar Position Algorithm developed by the National Renewable Energy Laboratory”. 21 Aug. 2017 <https://midcdmz.nrel.gov/spa/>.

Philibert, C., 2014. Technology roadmap: solar thermal electricity—2014 edition. IEA, Paris, France.

Reda, I. and Andreas, A., 2008 Solar Position Algorithm for Solar Radiation Applications.; NREL Report No. TP-560-34302, Revised January 2008.

Zarza, E., Valenzuela, L., Leon, J., Hennecke, K., Eck, M., Weyers, H.D. and Eickhoff, M., 2004. Direct steam generation in parabolic troughs: Final results and conclusions of the DISS project. Energy, 29(5), pp.635-644.

Zhu, G., Wendelin, T., Wagner, M.J. and Kutscher, C., 2014. History, current state, and future of linear Fresnel concentrating solar collectors. Solar Energy, 103, pp.639-652.

7. RESPONSIBILITY NOTICE

The authors are the only responsible for the printed material included in this paper.